

Modelling the inhalation of drug particles in a human nasal cavity

Kiao Inthavong, Jian Wen, Ji-Yuan Tu*

School of Aerospace, Mechanical and Manufacturing Engineering, RMIT University, Bundoora, Australia.

Email: jiyuan.tu@rmit.edu.au

Received 6 August 2009; revised 25 October 2009; accepted 27 October 2009.

ABSTRACT

A human nasal cavity was reconstructed from CT scans to make a Computational Fluid Dynamics (CFD) model. With this model, fluid flow and inhalation of aerosol analysis can be investigated. The surface of the interior nasal cavity is lined with highly vascularised mucosa which provides a means for direct drug delivery into the blood stream. Typical sprayed particles from a nasal spray device produce a particle size distribution with a mean diameter of 50 μm , which leads to early deposition due to inertial impaction. In this study low-density drug particles and submicron particles (including nanoparticles) are used to evaluate their deposition patterns. It was found that the low-density particles lightens the particle inertial properties however the particle inertia is more sensitive to the particle size rather than the density. Moreover the deposition pattern for nanoparticles is spread out through the airway. Thus an opportunity may exist to develop low-density and nanoparticles to improve the efficiency of drug delivery to target deposition on the highly vascularised mucosal walls.

Keywords: Nasal Airway; Ultrafine, Fibre; Morphology; CFD; Deposition

1. INTRODUCTION

Nasal drug delivery provides an alternative approach to traditional delivery methods such as oral drug routes that fail in the systemic delivery of compounds due to its dissociation by the digestive system. The nasal airway is dominated by the nasal turbinates that are lined with highly vascularised mucosa opening to the paranasal sinuses. Because of these characteristics it is hypothesised that drug delivery to combat health problems such as lung diseases, cancers, diabetes, sinus infections etc. may be viable if the drug formulation can be deposited in the turbinate region [1].

Despite these advantages, studies have found that tar-

geted drug delivery is inefficient [2,3]. The atomisation of the drug formulation produces a mean droplet size of 50 μm [4] which exhibits high inertia. This leads to a large proportion of particles impacting in the anterior regions of the nasal cavity. Most drug formulations have close to unit density as they are suspensions in aqueous solutions. Lighter porous drug particles have been developed for pulmonary delivery [5], where the drug particle sizes are in the low micron to sub-micron range and deposition is targeted at the pulmonary airways that exhibit much smaller spaces such as the airway branches in the lungs. Another alternative is the use of engineered nanoparticles which exhibit a large surface area to size ratio leading to greater biologic activity. This increased biologic activity can be exploited for targeted drug and gene delivery, tissue engineering, cell tracking and bio-separation [6,7]. One advantage for nasal drug delivery is its extremely small size which would allow the particles to deposit through diffusion rather than inertial impaction. Thus an opportunity exists for the development of new porous-based particles and/or nano-sized particles for nasal drug delivery.

Computational Fluid Dynamics (CFD) simulations have evolved into a feasible alternative to complement experimental data. For example CFD simulations for airflow patterns [8,9,10] have complemented experimental results [11] by confirming regions of vortices within the nasal vestibule, the olfactory region and posterior to the nasal valve. Simulations for particle deposition however, are fewer in numbers. Spherical particle deposition under conditions related to pharmaceutical nasal spray applications has been studied [3]. Particles in the range of 10 μm to 50 μm subjected to a breathing flow rate of 20L/min found that a large proportion of particles deposited in the anterior third of the nasal cavity which were attributed to the injected particles existing in a high inertial regime. On the other hand nano-sized particles in the nasal cavity under laminar conditions were simulated [12] which found that diffusion was the dominant deposition mechanism for the smallest range of particles (1–30 nm).

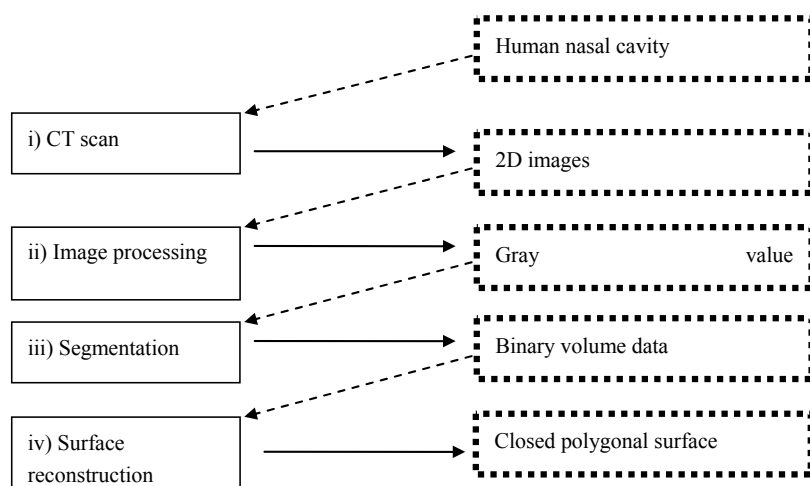


Figure 1. Steps in the construction of the computational model.

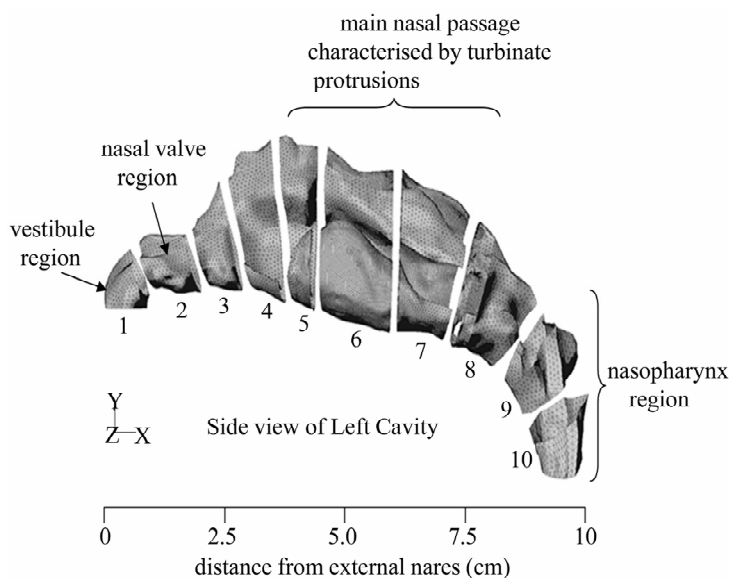


Figure 2. Different views of the computational model. Three coronary slices and the inlet show the internal mesh with a dense region near the walls.

A human nasal cavity was reconstructed from CT scans and a computational model developed for particle flow analysis within the airway. This study presents the use of CFD techniques to investigate the airflow patterns and deposition of low density and nano-sized particles for drug delivery in a human nasal cavity. The nasal airway was chosen for investigation as it is one of the major entries into the respiratory system which can be penetrated to reach the blood streams. With this in mind, it is anticipated that this research will assist in new designs of aerosols and particulates and also help to guide practical clinical tests for toxicological and therapeutic studies.

2. METHOD

The model reconstruction involved four main steps

(**Figure 1**): 1) CT images acquisition; 2) image processing and editing to improve the quality of the image volume; 3) segmentation; and 4) surface reconstruction. CT images of a 25 yr-old Asian male (75kg, 170cm) provided a 3D matrix of volume elements (voxels), in which different tissues and structures having different attenuation characteristics were distinguished from one another by differences in brightness or greyscale.

2.1. Image Processing

The scan was performed using a CTI Whole Body Scanner (General Electric). The single-matrix scanner was used in helical mode with 1-mm collimation, a 40-cm field of view (FOV), 120 kV peak and 200 mA to produce contiguous images (slices) of 1-mm thickness



Figure 3. Path streamlines in the left and right cavities.

with voxel size $0.25 \times 0.25 \times 1$ mm. The original set of CT images is converted into a file format compatible with the package MegaWave2 (MW2), by means of C language self-developed routines. The conversion program also performs an image enhancement, by rescaling the grey-level histogram to 1-200 and remapping the image volume to an 8-bit/pixel depth file.

A 3D convolution with a Gaussian kernel was used to reduce the background noise present in the images. Because of its isotropic shape, the Gaussian filter has optimal properties such as smoothing mask, removing small-scale texture and noise, which could alter the regional segmentation, without distorting lower spatial frequencies. Filtering was applied in three dimensions in order to obtain a smoothed CT image volume also along the axial direction. Such a procedure attenuates the spatial discontinuities among the slices introduced during acquisition, as an effect of the slice thickness.

2.2. Segmentation & Surface Reconstruction

A 2D segmentation is used to detect and extract, slice by slice, the walls of the airway. For the segmentation process, a region growing algorithm, based on the Mumford and Shah [13] method implemented WM2 is used. The regional segmentation has been included because it allows the tracking only of the domains of interest, even in the presence of noise. A first regional segmentation with a greater number of partitioning regions than necessary is performed on each single slice. This allows the algorithm to detect the walls even in severely disturbed images. A threshold binarisation process is then applied in order to remove sub-regions unrelated to the airway, which typically present a lower intensity value with respect to the signal. In this work, the threshold has been empirically chosen and represents 45% of the maximum grey-level value of the study. Generation of a surface or solid model from the 2D contour data began with the translation of the segmented, modified and smoothed contour points into a data series that was read into CAD package used in this study: CATIA. The contours were lofted to define surface splines which enclosed the airway volume.

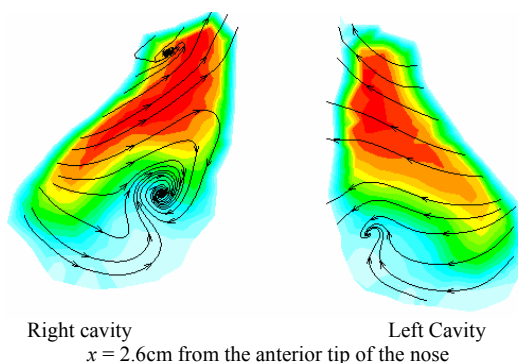


Figure 4. Contour plot of axial velocity (x -velocity) combined with cross flow path streamlines (y - z velocity) in the left and right cavities.

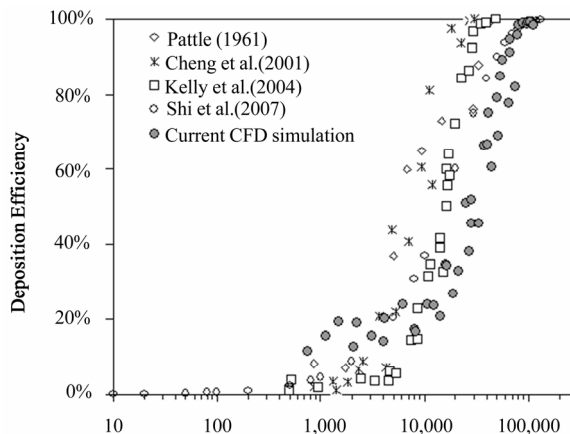


Figure 5. Deposition efficiency vs inertial parameter comparisons for the simulation micron spherical particles.

2.3. Adaptive Meshing

The CATIA models were imported into a 3D modelling program called GAMBIT. An initial model with 82,000 cells was created and used to solve the air flow field at a flow rate of 7.5 L/min. The original model was refined by cell adaptation techniques that included refining large volume cells, cells that displayed high velocity gradients and near wall refinements. This process was repeated twice, with each repeat producing a model with a higher

cell count than the previous model. Subsequently four models were produced, 82000, 586000, 950000 and 1.44 million cells. A grid independence test found that the results for average velocity converged at 950,000 cells. Subsequently the 950,000 cell model was used and is shown in **Figure 2**.

2.4. Numerical Method

Due to the complex geometry of the anatomically real nasal cavity a commercial CFD code, FLUENT, was used to predict the continuum air phase flow through solutions of the conservation equations of mass and momentum. The steady continuity and momentum equations for the gas phase (air) in Cartesian tensor notation are:

$$\frac{\partial}{\partial x_i}(\rho_g u_i^g) = 0 \tag{1}$$

$$\rho u_j^g \frac{\partial u_i^g}{\partial x_j} = -\frac{\partial p_g}{\partial x_i} + \frac{\partial}{\partial x_j} \left(\mu_g \frac{\partial u_i^g}{\partial x_j} \right) \tag{2}$$

where u_i^g is the i -th component of the time averaged velocity vector and ρ_g is the air density. These equations were discretised using the finite volume approach. The third order accurate QUICK scheme was used to approximate the momentum equation whilst the pressure-velocity coupling was realized through the SIMPLE

method. To be consistent with experimental data, a constant flow rate of 7.5 L/min. was used to simulate light breathing. At this flow rate, the flow regime has been determined to be laminar [11,14]. A steady flow rather than a cyclic unsteady flow was used in this case to allow the results to emphasize the effects of particle morphology on deposition sites independent from cyclic conditions. Moreover the effects of a periodic inhalation on the overall flow field are found to be negligible from the Womersley frequency variable which is used to determine the importance of the fluctuating sinusoidal pattern of the inhalation-exhalation breathing cycle. The Womersley frequency variable,

$$W = D/2(\omega/\nu_g)^{0.5} \tag{3}$$

was calculated as 0.3 where D is the local cross-sectional distance between the two nasal walls and is about 0.5 cm in this nasal cavity, ν_g is the kinematic viscosity of air and ω is the breathing frequency.

2.5. Drug Particles

For spherical particles the drag force is related to the drag coefficient which has been studied quite extensively. The general correlation for smooth spherical particles is given as [15]:

$$C_D = 24/18 Re_p (18 + 2.367 \cdot Re_p^w) \text{ for } Re < 20 \tag{4}$$

Table 1. Deposition efficiency based on **Figure 5**.

Density	d_{ac}	Inertial Parameter (IP)	Deposition % present simulation
100	15.8	41,667	67.4%
200	22.4	83,333	95.3%
1000	50.0	416,667	100%

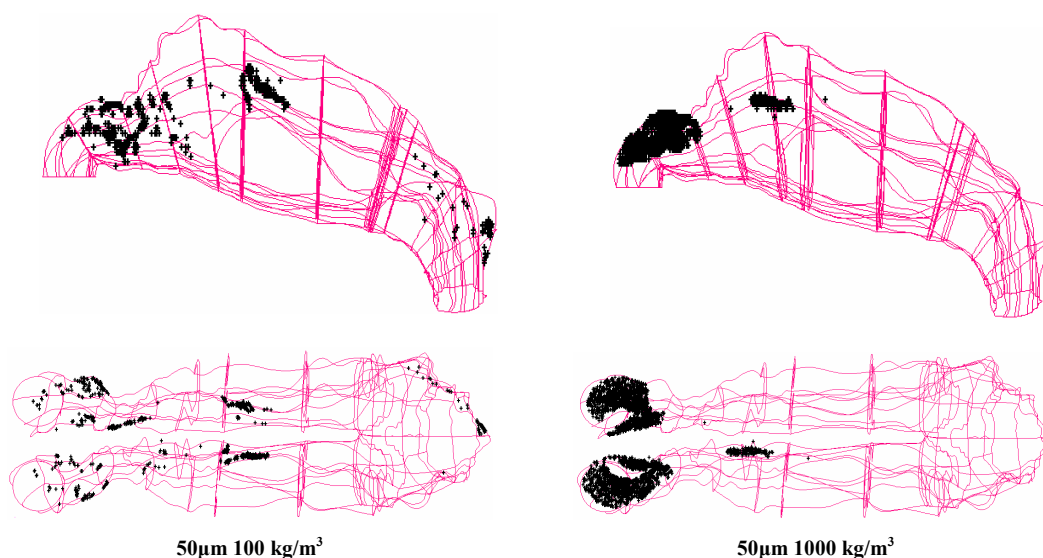


Figure 6. Deposition pattern for low density particles where $\rho = 100\text{kg/m}^3$ and 1000kg/m^3 .

where $w = 0.82 - 0.05(\log_{10} Re_p)$

For submicron particles the drag force per unit particle mass taking the form of Stokes' drag law [16] defined as,

$$F_D = \frac{18\mu}{d_p^2 \rho_p C_c} (u_i^s - u_i^p) \quad (5)$$

C_c is the Cunningham correction factor to Stokes' drag law. The Brownian force by Li and Ahmadi [17] can be re-arranged to highlight the diffusion coefficient as:

$$F_B = \frac{\zeta}{m_d} \sqrt{\frac{1}{\tilde{D}} \frac{2k_B^2 T^2}{\Delta t}} \quad (6)$$

where m_d is the mass of the particle, T is the absolute temperature of the fluid, ν is the kinematic viscosity, k_B is the Boltzmann constant, and \tilde{D} is the diffusion coefficient. Eq.6 is inputted into the user-defined-function option in Fluent. Additional forces include Saffman's lift force [18]

$$F_L = \frac{2K\nu^{1/2} \rho d_{ij}}{\rho_p d_p (d_{ik} d_{kl})^{1/4}} (\bar{v} - \bar{v}_p) \quad (7)$$

and the thermophoretic force [19]

$$F_T = -D_T \frac{1}{m_p T} \frac{\partial T}{\partial i} \quad (8)$$

Particle rebounding from the surfaces was ignored and particle deposition was determined when the distance between the particle centre and a surface was less than or equal to the particle radius.

3. RESULTS AND DISCUSSION

3.1. Airflow Patterns

Path streamlines which act as massless particle tracers to track the flow path of the inhaled air, were released from the nostril inlet to provide visualisation of the flow field (Figure 3). The streamlines in the left nasal cavity at a flow rate of 7.5L/min show flow separation and reversed flow in the upper anterior part of the cavity (olfactory region). This low flow characteristic in the olfactory region is important as it is a defence mechanism that prevents particles whose trajectories are heavily dependent on flow patterns from being deposited onto the sensitive olfactory nerve fibres, while vapours are allowed to diffuse for olfaction. For both cavities, the air flow squeezes through the nasal valve region, before decelerating due to the expansion in the cross-sectional area. The nasal valve region is approximately 2cm from the nostril inlet.

A cross-sectional area located just immediate of the anterior nasal valve at 2.6cm was chosen to reflect the rapid changes in the flow field. The cross-section shown

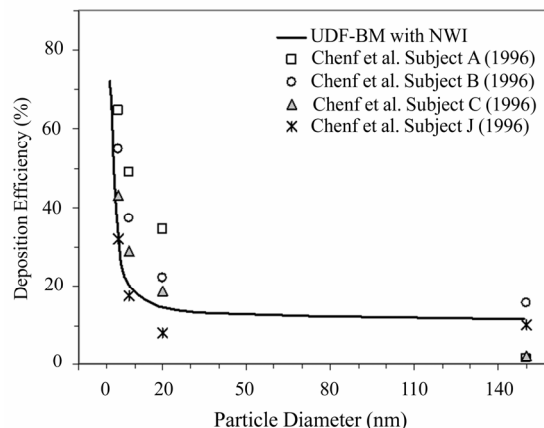


Figure 7. Deposition efficiency of 1nm-150nm particles in a human nasal cavity at a steady inhalation rate of 10L/min.

in Figure 4 is from a frontal perspective (positive flow into the paper). The contours reflect the axial velocity (x -component of velocity) and are combined with streamlines of secondary flow (y - z component of velocity). The red contours are maximum values which represent the bulk flow regions. For the cross-section located at 2.6cm from the anterior tip of the nose, two vortices in the right cavity and one in the left are found. The bulk flow is found in the middle and upper regions of the both cavities.

3.2. Deposition of Drug Particles

A parameter used for normalizing impaction-dominant deposition studies is the inertial parameter, IP given by:

$$IP = Qd_{ae}^2 \quad (9)$$

where Q is the air flow rate, given in cm^3/s and d_{ae} is the aerodynamic diameter given in μm . It is a convenient parameter that compares deposition against different flow rates and particle sizes at aerodynamic diameters. Monodispersed particles in the range of 1-30 μm were released passively (with the airflow) into the nasal cavity at flow rates of 5, 7.5, 10 and 15L/min. The deposition of particles over a range of the inertial parameter is shown in Figure 5 and is compared with other experimental results.

Since the drug particles exhibit different densities, they can be compared in terms of their aerodynamic properties (inertia, and settling properties) through the equivalent aerodynamic diameter, d_{ae} defined as:

$$d_{ae} = d_p \sqrt{\rho_p / 1000} \quad (10)$$

This means that a small diameter, very dense particle can have the same aerodynamic as a large diameter, but less dense particle if their d_{ae} are the same.

Particles in the micron particle size range exist in the inertial regime where deposition by inertial impaction is

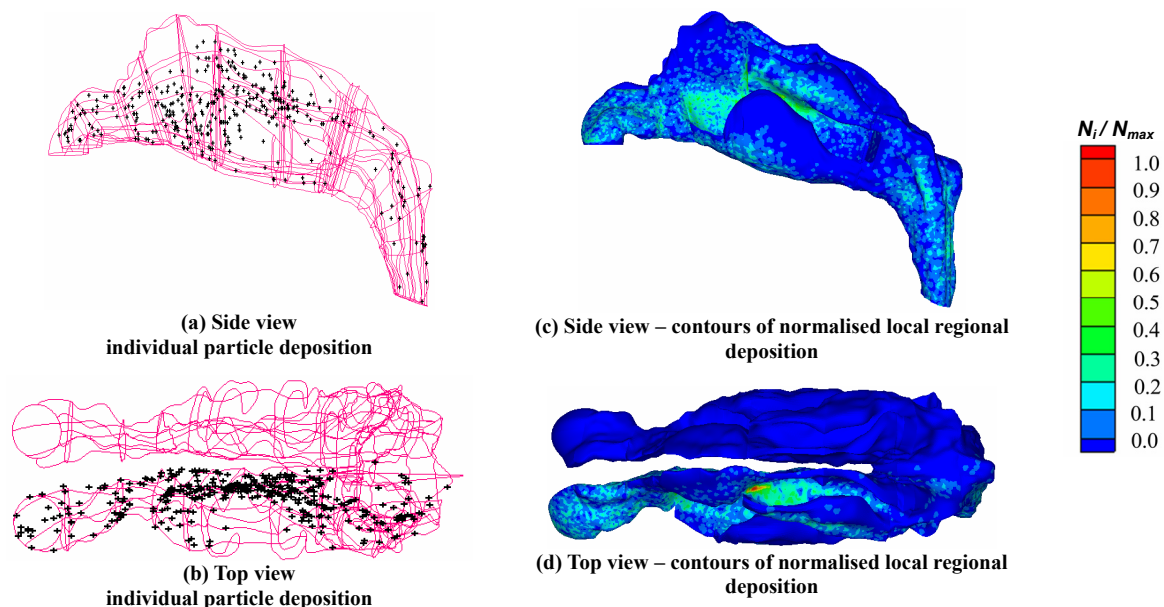


Figure 1. Regional deposition patterns of 1nm particles under a flow rate of 10L/min in a human nasal cavity.

relevant. The idea of low-density porous drug particles will decrease the particle inertial properties, although this decrease is not as significant as changing the particle size. The inertial parameter incorporates both the geometric equivalent spherical diameter along with the particle density to give the particle aerodynamic diameter (Eq.12). Thus a larger porous particle will have a smaller equivalent aerodynamic diameter than a particle of equal size but with a higher density. The effect of particle density on the deposition of a $50\mu\text{m}$ particle is shown below.

The particle deposition patterns in the nasal cavity in **Figure 6** shows particles with density of 100kg/m^3 and 1000kg/m^3 for brevity as the deposition pattern for $\rho = 200\text{kg/m}^3$ becomes similar to that of $\rho = 100\text{kg/m}^3$. For particles with densities of 100kg/m^3 a portion of the particles deposit superiorly on the septum walls of both sides of the nasal cavity. This suggests that the fluid flow is close to the inner septum walls forcing the particles into this region.

A second concentration of deposited particles occurs at the back of the nasal cavity where the flow changes directions from horizontal to vertically downwards. The change in the flow direction causes the particles to impact in this region. For particles with density of 1000kg/m^3 deposition is found in the frontal area with only a small proportion of particles passing through the nasal valve region. These particles finally impact onto the superiorly on the septum wall of the left nasal cavity, however this pattern is not found in the right nasal cavity.

Deposition of submicron particles (1 to 150nm) was simulated under a flow rate 10 L/min in order to make

comparisons with experimental data reported by [20] which found deposition efficiencies for a variety of human subjects under a flow rate of 10 L/min. The solid line in **Figure 7** corresponds to the CFD model prediction. The deposition curve is high for very small nanoparticles and the particle diameter range in which the deposition drops from 72% to 18% is between 1nm-10nm. From 10nm-150nm however, there is only a small change in the deposition curve from 18%-15%. This deposition curve profile is characteristic of the Brownian diffusion, where the particles are so small that the fluid may no longer be considered continuous. The trajectory of the nanoparticle is then caused by the collision of the air molecules and concentration gradients to produce the random motion.

Local deposition patterns for a 1nm particle are shown in **Figure 8**. The deposition pattern of the 1nm particle is distributed evenly through the nasal cavity where the diffusion disperses the particles in all directions. The wall contours in **Figure 8(c), (d)** show regions of high concentrations which is determined by the number of particles that deposit onto a wall face divided the maximum number of particles that deposit on any one face. Few particles are able to reach the wider meatus region, and instead the particles remain close to the nasal septum wall (inner regions). High concentrations are found at the upper regions of the cavity with a higher distribution of deposition within that one area.

In general the deposition pattern is spread out through the nasal cavity well. This has interesting applications for drug delivery where traditional nasal sprays are producing micron sized droplets that are prone to inertial deposition. This deposition mechanism leads to high

inertial impaction (up to 100% for a mean atomised particle droplet of 50 μ m) in the anterior region of the nasal cavity [2,3]. However for high drug efficacy, the delivery of the droplets needs to be deposited in the middle regions of the nasal cavity, where the highly vascularised walls exist. Smaller particles such as 1 μ m were found to be less affected by inertial properties, which allowed it to bypass the anterior region of the nasal cavity. However because of the particles ability to follow the streamlines more readily, the particles were less likely to deposit in any region of the nasal cavity and instead bypasses it completely, leading to the undesired effects of lung deposition. Delivery of nanoparticles especially 1nm-5nm particles therefore, can provide improved deposition in the middle regions whilst minimising deep lung deposition.

4. CONCLUSIONS

Simulations of air-particle flows in the nasal cavity found vortices primarily in the upper olfactory region and just posterior to the nasal valve where the geometry begins to expand. This suggests that high inertial particles are unlikely to reach the sensitive olfactory region. Multiple secondary flow regions were found in the lower middle regions within the nasal valve. Low density porous drug particles lightens the particle inertial properties however the particle inertia was more sensitive to the particle diameter rather than its density. The deposition of nanoparticles in the nasal cavity was distributed evenly throughout the airway with a deposition that drops from 72% to 18% for 1nm to 10nm. Because of the evenly distributed deposition pattern for nanoparticles there exists an opportunity to develop low-density and nanoparticles to improve the efficiency of drug delivery to target deposition on the highly vascularised mucosal walls.

5. ACKNOWLEDGEMENTS

The financial support provided by the Australian Research Council (project ID LP0989452) and by RMIT University through an Emerging Research Grant are gratefully acknowledged.

REFERENCES

- [1] Kimbell, J., Shroeter, J.D., Asgharian, B., Wong, B.A., Segal, R.A., Dickens, C.J., Southall, J.P. and Millerk F. J. (2004) Optimisation of nasal delivery devices using computational models. *Res. Drug Del.*, **9** 233-238.
- [2] Inthavong, K., Tian, Z.F., Tu, J.Y., Yang, W. and Xue, C. (2008) Optimising nasal spray parameters for efficient drug delivery using computational fluid dynamics. *Computers in Biology and Medicine*, **38**(6), 713-726.
- [3] Inthavong, K., Tian, Z.F., Li, H. F., Tu, J.Y., Yang, W., Xue, C.L. and Li, C.G. (2006) A numerical study of spray particle deposition in a human nasal cavity. *Aerosol Science Technology*, **40**, 1034-1045.
- [4] Cheng, Y.S., Holmes, T.D., Gao, J., Guilmette, R.A., Li, S., Surakitbanharn, Y. and Rowlings, C. (2001) Characterization of nasal spray pumps and deposition pattern in a replica of the human nasal airway. *J. Aerosol Medicine*, **14** (2), 267-280.
- [5] Edwards, D.A., Hanes, J., Caponetti, G., Hrkach, J., Ben-Jebria, A., Eskew, M.L., Mintzes, J., Deaver, D., Lotan, N. and Langer, R. (1997) Large porous particles for pulmonary drug delivery. *Science*, **276**, 1868-1872.
- [6] Gupta, A.K. and Gupta, M. (2005) Synthesis and surface engineering of iron oxide nanoparticles for biomedical applications. *Biomaterials*, **25**(18), 3995.
- [7] McCarthy, J.R., Kelly, K.A., Sun, E.Y. and Weissleder, R. (2007) Targeted delivery of multifunctional magnetic nanoparticles. *Nanomedicine*, **2**(2), 153-167.
- [8] Keyhani, K., Scherer, P.W. and Mozell, M.M. (1995) Numerical simulation of airflow in the human nasal cavity. *J. Biomechanical Engineering*, **117**, 429-441.
- [9] Subramaniam, R.P., Richardson, R.B., Morgan, K.T., Kimbell, J.S. and Guilmette, R.A. (1998) Computational fluid dynamics simulations of inspiratory airflow in the human nose and nasopharynx. *Inhalation Toxicology*, **10**, 91-120.
- [10] Finckl M.H. and Wlokas, D.I. (2006) Simulation of nasal flow by lattice Boltzmann methods. *Computers Biology Medicine*, **37**(6), 739-749.
- [11] Hahn, I., Scherer, P.W. and Mozell, M.M. (1993) Velocity profiles measured for airflow through a large-scale model of the human nasal cavity. *J Appl. Physiol.*, **75**(5), 2273-2287.
- [12] Zamankhan, P., Ahmadi, G., Wang, Z., Hopke, P.H., Cheng, Y.S., Su, W.C. and Leonard, D. (2006) Airflow and deposition of nanoparticles in a human nasal cavity. *Aerosol Science Technol.*, **40**, 463-476.
- [13] Mumford, D. and Shah, J. (1989) Optimal approximations by piecewise smooth functions and associated variational problems. *Communications Pure and Applied Mathematics*, **XLII**, 577-685.
- [14] Swift, D.L. and Proctor, D.F. (1977) Access of air to the respiratory tract., in *Respiratory Defence Mechanisms.*, Brain, J.D., Proctor, D.F. and Reid, L.M. Editors, Marcel Dekker, New York, NY, 63-93.
- [15] Clift, R., Grace, J.R. and Weber, M.E. (1978) Bubbles, Drops, and Particles. London, Academic Press Inc, UK, London, Ltd.
- [16] Ounis, H., Ahmadi, G.M.J.B., (1991) Brownian diffusion of submicrometer particles in the viscous sub-layer. *J. Colloid and Interface Science*, **143**(1), 266-277.
- [17] Li, A. and Ahmadi, G. (1992) Dispersion and deposition of spherical particles from point sources in a turbulent channel flow. *Aerosol Science Technology*, **16**, 209-226.
- [18] Saffman, P.G. (1965) The lift on a small sphere in a slow shear flow. *J. Fluid Mechanics*, **22**, 385-400.
- [19] Talbot, L., Cheng, R.K., Schefer, R.W. and Willis, D. R. (1980) Thermophoresis of particles in a heated boundary layer. *J. Fluid Mech*, **101**(4), 737-758.
- [20] Cheng, K.H., Cheng, Y.S., Yeh, H.C., Guilmette, A., Simpson, S.Q., Yang, Y.H. and Swift, D.L. (1996) *In-vivo* measurements of nasal airway dimensions and ultrafine aerosol deposition in the human nasal and oral airways. *J. Aerosol Science*, **27**(5), 785-801.